Modular 'Click-in-Emulsion' Bone-Targeted Nanogels

Published in final edited form as:
Adv Mater. 2013 March 13; 25(10): . doi:10.1002/adma.201202881.

Modular 'Click-in-Emulsion' Bone-Targeted Nanogels

Daniel A. Heller[1,2,3,#], **Yair Levi**[1,2,4,#], **Jeisa M. Pelet**[1,2,4,#], **Joshua C. Doloff**[1,2,4], **Jasmine Wallas**[1,2,3,4], **George W. Pratt**[1,2,4,5], **Shan Jiang**[1,2], **Gaurav Sahay**[1,2], **Avi Schroeder**[1,2,4], **Josh E. Schroeder**[6], **Yieu Chyan**[1], **Christopher Zurenko**[7], **William Querbes**[7], **Miguel Manzano**[1,8,9], **Daniel S. Kohane**[8], **Robert Langer**[1,2,10], and **Daniel G. Anderson**[1,2,4,10,*]

[1]David H. Koch Institute for Integrative Cancer Research, Massachusetts Institute of Technology, Cambridge, MA

[2]Department of Chemical Engineering, Massachusetts Institute of Technology, Cambridge, MA

[3]Molecular Pharmacology and Chemistry Program, Memorial Sloan-Kettering Cancer Center, New York, NY

[4]Department of Anesthesiology, Children's Hospital Boston, Boston, MA

[5]Department of Bioengineering, Boston University, Boston, MA

[6]Department of Orthopedic Surgery, Hospital for Special Surgery, New York, NY

[7]Alnylam Pharmaceuticals, Inc., Cambridge, MA

[8]Laboratory for Biomaterials and Drug Delivery, Department of Anesthesiology, Division of Critical Care Medicine, Children's Hospital Boston, Harvard Medical School, Boston, MA

[9]Departamento de Química Inorgánica y Bioinorgánica, Facultad de Farmacia, Universidad Complutense de Madrid, Spain

[10]Division of Health Science Technology, Massachusetts Institute of Technology, Cambridge, MA

Abstract

A new class of nanogel demonstrates modular biodistribution and affinity for bone. Nanogels, 67 nm in diameter and synthesized via an astoichiometric click-chemistry-inemulsion method, controllably display residual, free click-able functional groups. Functionalization with a bisphosphonate ligand results in significant binding to bone on the inner walls of marrow cavities, liver avoidance, and anti-osteoporotic effects.

Keywords

Nanotechnology; Drug delivery; Polymers; Nanogel; Bone

A new class of nanogel with controllable surface functionalization was developed and employed for targeting bone, demonstrating modular biodistribution and affinity for the marrow-bone interface. Nanogels, 67 nm in diameter and composed of dextran, were synthesized via an astoichiometric click-chemistry-in-emulsion method to controllably display residual, free click-able functional groups. Following intravenous injection in mice, nanogels localized in cervical lymph nodes, liver, and the bone marrow cavities, observed in

[*]Contact: dgander@mit.edu.
[#]These authors contributed equally

((Supporting Information is available online from Wiley InterScience or from the author)).

the spine and femur. Functionalization of nanogels with a bisphosphonate ligand modulated this localization, reducing liver uptake by 43% and effecting localization on the marrow-bone interface. The targeting ligand resulted in significant nanogel binding to hydroxapatite (HA) molecules on the inner walls of the marrow cavity in both cortical and trabecular bone and reduced nanogel uptake into bone marrow F4/80-positive cells. Targeted nanogels also depleted F4/80-positive cells within bone marrow, suggesting anti-osteoporotic effects.

Bone diseases, such as osteoporosis, metabolic diseases, and metastatic cancers, are common, but systems capable of targeting therapeutics to the bone remain limited.[1] Nanogels—porous nanoscale hydrogel networks, are a class of nanomaterials with tunable chemical properties that facilitate targeting and delivery to specific tissues. They are intrinsically porous and can be loaded with small drugs or macromolecules by physical entrapment, covalent conjugation or controlled self-assembly.[2]

Nanogels based on biopolymers potentially benefit from their low toxicity and biorecognitive properties. Dextran, a polysaccharide of glucose, can be recognized by C-type lectin receptors in myeloid cells and taken up by these cells.[3] Crosslinked nanogels composed primarily of dextran have been synthesized and usually contain other polymeric building blocks, such as hydroxyl ethyl methacrylate, used for free radical polymerization.[4] Biodistribution of nanogels appears to be modulated in part by the attachment of surface ligands, similar to behavior of other nanoparticle types. For instance, the functionalization of poly(2-N,N-(diethylamino)ethyl methacrylate) nanogels with polyethylene glycol (PEG) results in a shift of distribution from the liver and spleen towards the lungs and kidneys.[5] Nanogels incorporating dextran have shown promise as delivery vehicles,[4] however little related in vivo work has been conducted, and no such work has been shown in bone tissue.

The high concentration of the mineral hydroxyapatite (HA) in bone represents a promising target for selective delivery. Calcium ions in HA are chelated by the bisphosphonate (BP) group, which is structurally analogous to endogenous inorganic phosphate.[6] Systemic administration of BPs leads to deposition of these molecules on bone tissues with minimal accumulation at other sites.[7] Bisphosphonates are used to treat osteoporosis, metabolic diseases,[8] and they have been explored for the targeting of radiopharmaceuticals, estrogen, corticoids, anti-inflammatory agents, and proteins.[1, 9] Polymers targeted with bisphosphonate ligand have demonstrated bone tissue localization.[10]

Herein, we introduce a facile method to produce nanogels using click chemistry[11] with free groups for surface modification which we employed to target several tissues, including bone. The biopolymer dextran, modified separately with clickable alkyne or azide groups, was crosslinked within an inverse emulsion to result in nanoparticles with an excess of free unreacted groups for subsequent conjugation. Both free click-able groups were used to control the nanogel surface and internal properties. The nanogels, with an average diameter of 67 nm, were characterizable via NMR, underwent enzymatic degradation, exhibited negligible cytotoxicity, and demonstrated preferential uptake by macrophages in vitro. In vivo biodistribution studies found that dextran nanogels localized in lymph nodes, liver, spine and femur. Moreover, the bisphosphonate ligand reduced nanogel uptake in the liver by 43%. While non-targeted nanogels entered the bone marrow and were engulfed by F4/80-positive cells in this tissue, bisphosphonate-functionalized nanogels exhibited reduced F4/80-positive cell uptake and demonstrated binding to both cortical and trabecular bone lining the marrow cavities. Although the over all uptake into the F4/80-positive cells decreased, a secondary benificial effect was noted by F4/80-postive cell depletion, suggesting an anti-osteoporotic capacity of the targeted nanogels.

Nanogels composed of dextran were synthesized by initiating click chemistry within an inverse emulsion and characterized by several methods. Dextran polysaccharide (MW = 10,000 Da) was modified via conjugation separately with a ligand bearing an alkyne group or azido group (Figure 1a). The alkyne-functionalized dextran (alkyne-dextran), characterized via NMR (Figure S1 and Supporting Experimental Methods), was synthesized with an alkyne ligand substitution ratio of 11.7% per glucose subunit, while azide-dextran exhibited a 4.6% substitution ratio (calculations described in methods).

The nanogel particles were assembled by clicking the two modified dextran polymers together in either a 3:1 or 1:3 alkyne-dextran:azide-dextran ratio within an inverse emulsion,[12] producing alkyne-heavy or azide-heavy particles respectively (Figure 1b). The alkyne-azide cycloaddition reaction between substituted dextrans was initiated with Cu^{+2} and sodium ascorbate added to the aqueous phase before emulsification with cyclohexane and a lipophilic surfactant. The resulting nanogels were characterized by NMR upon dispersing in deuterated water after purification. The spectra (Figure S1) exhibit diminished alkyne peaks and allow quantification of the remaining excess alkyne groups. The alkyne-heavy particles contain a final alkyne ligand substitution ratio of 7.4% with respect to the total number of glucose subunits contained in the particle. The NMR spectra show negligible azido group signal within both alkyne-heavy and azide-heavy nanogels, possibly due to low intrinsic signal strength of the group or restricted ligand mobility due to preferential localization within the particle instead of on the surface.[13]

Dynamic light scattering (DLS) measurements of nanogels dispersed in PBS exhibit mean diameters of 67 nm and 86 nm for alkyne-heavy and azide-heavy particles, respectively, suggesting relatively monodisperse particle sizes (Figure 1c). Transmission electron micrographs (TEM) of alkyne-heavy nanogels show particles of homogenous electron densities with sizes between 20 and 40 nm (Figure 1d–e). These differences between size measurements in aqueous medium (DLS) and dry (electron microscopy) are consistent with other nanogel types.[14]

Nanogels were imaged by atomic force microscopy (AFM) to confirm formation of crosslinked particles. Silicon functionalized with an azido-silane compound (6-azidosulfonylhexyl-triethoxysilane) was used to promote alkyne-heavy nanogel attachment via cycloaddition conducted on the silicon surface. Height measurements, conducted in air, show evidence of surface-adsorbed spherical particles which confirm the sizes observed in the TEM micrographs (Figure 1f–g).

The nanogels showed evidence of enhanced degradation in the presence of dextranase. The nanogels, kept in pH 6.0 buffer to maximize dextranase efficiency, swelled to approximately 500% of their original size within 6 days of dextranase introduction (Figure 2a). This behavior is consistent with other investigators' nanogel systems which demonstrate swelling as a result of the degradation of intra-particle crosslinks.[15] Particles in dextranase-free buffer exhibited comparatively slight swelling behavior.

The astoichiometric excess of alkyne or azido groups allowed nanogel post-functionalization with two different moieties. Alkyne-heavy nanogels were functionalized with a bisphosphonate-presenting group containing a labile azido moiety, synthesized from alendronate precursor. The bisphosphonate-functionalized nanogels exhibited little change in size compared to unfunctionalized alkyne-heavy nanogels (Figure 1c), with a peak diameter averaging 69 nm. The minority clickable group was also present in the nanogels and used for functionalization with a second ligand. The azido group in alkyne-heavy nanogels, although undetected by NMR spectroscopy, was functionalized with Alexa Fluor 647 containing an alkyne moiety and resulted in fluorescent nanogels post purification. The

nanogels contained approximately 0.3 nmol of fluorophore per milligram of particles according to absorption spectrophotometry. Bi-functionalized nanogels exhibiting both fluorophore and bisphosphonate ligands contained 0.19 nmol of fluorophore per milligram of particle.

A binding study demonstrates that bisphosphonate functionalization increases nanogel affinity to the bone mineral hydroxyapatite (Figure 2b–d). Hydroxapatite, adhered to a polystyrene surface, was interrogated with either dextran nanogels or bisphosphonate-functionalized nanogels. Both nanogel constructs were conjugated to Alexa Fluor 647 fluorescent dye using their minor (azido) clickable group. After 12 hours of incubation, bisphosphonate-labeled nanogels exhibited significantly higher binding to hydroxyapatite, as demonstrated by a 23% higher emission intensity on the hydroxyapatite particles, relative to alkyne-heavy nanogels, quantified by normalizing mean fluorescence to the hydroxyapatite-covered area.

Dextran nanogels demonstrated higher uptake by macrophages than epithelial cells and hepatocytes in vitro, and they exhibited negligible cytotoxicity in all studied cell types. RAW264.7 cells (murine macrophage cell line) showed a 4-fold increase in uptake of Alexa Fluor 647-labeled nanogels as compared to HeLa or hepatocellular carcinoma (HepG2) cell lines (Figure 3a). In vitro measurements, collected in a 96-well plate format via high-throughput confocal microscopy, resulted in over 90 images of confluent cells under each condition. The images were processed in order to measure total corrected fluorescence intensity per cell (Figure 3b). Bisphosphonate functionalization in nanogels attenuated cellular uptake by RAW264.7, as suggested by the 40% reduction in fluorescent intensity. Still, the fluorescent signal in these cells remained significantly higher than in HeLa and HepG2 cell lines. Nanogel-mediated cytotoxicity was evaluated using the MTS assay. For non-functionalized nanogels, no measurable cell death was apparent in RAW264.7, HeLa and HepG2 cell lines even at concentration as high as 1.8 mg/mL (Table S1). Functionalization of bisphosphonate moieties in nanogels had a slight effect on cytotoxicity, particularly in Raw264.7 and HeLa cells, which showed IC_{50} values of 1.2 mg/mL and 1.5 mg/mL, respectively.

In vivo, bisphosphonate-functionalized nanogels exhibited spinal localization and attenuation of liver accumulation in murine biodistribution studies. Hairless SKH-1 mice were intravenously (i.v.) injected via the tail vein with a single dose of Alexa Fluor 647-labeled nanoparticles that were either un-functionalized or derivatized with a bisphosphonate ligand (100 μL; 75 mg/kg body weight). In vivo imaging of mice harboring alkyne-heavy nanogels showed generalized fluorescence in the body 24 hrs post-injection (Figure 4a; All mice shown in Figure S2). In the ventral view, a bright central fluorescent accumulation is apparent in the liver. In addition, pairs of fluorescent spots appear symmetrically at locations known to harbor cervical lymph nodes.[16] The dorsal image shows some generalized fluorescence throughout the body with localization in the body midsection and the centerline up to the head. For comparison, un-crosslinked dextran polymer demonstrates similar lymph node and centerline accumulation without liver localization (Figure S3). Of note, five days post-injection of dextran nanogels, the in vivo whole-body fluorescence attenuates markedly (Figure S4). Mice injected with bisphosphonate-functionalized nanoparticles exhibit attenuated fluorescence in the liver compared to non-functionalized dextran nanoparticles. Dorsally, the mice exhibit a higher relative localization of fluorescence up the centerline of the animal, especially at the midsection where the spine curves away from internal organs.

Imaging of the harvested organs confirms spinal accumulation, as well as liver and kidney attenuation, of bisphosphonate-functionalized nanoparticles compared to non-functionalized

dextran nanoparticles (Figure 4b, S5). Fluorescence quantification of whole organs by near-infrared imaging, shown to closely approximate other techniques,[17] was conducted 24 hrs after i.v. injection. Accumulation in femur for both types of nanoparticle is also appreciable and, notably, contrasts with whole-animal imaging data which shows little apparent accumulation. In mice treated with bisphosphonate-functionalized nanoparticles, corrected fluorescent intensity significantly decreases in liver and kidneys by approximately 43% for each organ. Localization increases slightly in the spleen, and significantly in the spine, by 36%. Overall, incorporation of the bisphosphonate moiety induces significant modulation in nanogel biodistribution, which are not attributable to changes in particle size or charge alone.

Dextran nanogels exhibited F4/80-positive cell uptake in femoral and spinal bone marrow, while bisphosphonate-functionalized nanogels attenuated this phenomenon, as shown by flow cytometry analysis. Bone marrow cells from femur and spine, harvested from Alexa Fluor 647-labeled dextran nanogel-treated mice, were labeled with FITC-conjugated F4/80 antigen-specific antibodies which target macrophages and osteoclast precursors.[18] For un-functionalized nanogels, flow cytometry measurements showed cells that are double positive for F4/80 and nanogels (4.12% cells for spine and 5.76% cells for femur), suggesting nanogel uptake by F4/80-positive cells (Figure 4c). Bone marrow cells from Alexa 647-labeled, bisphosphonate-functionalized nanogel treated mice showed near-background levels of nanogel emission. Cells which were double positive for F4/80 and bis-nanogels were reduced to 2.22% cells for spine and 3.14% cells for femur. This treatment group also showed lower total levels of F4/80-positive cells, likely denoting a depletion of F4/80-positive cells relative to the control. Depletion of macrophages and future osteoclasts, an effect of bisphosphonate, is described in the literature as the mechanism of its anti-osteoporotic effects.[19],[20] Furthermore, engulfment of nanogels by F4/80-positive cells was incomplete in the case of both dextran and bisphosphonate-modified nanogels, as many free nanogels were found within both the femoral and spinal marrow stroma, as detected by bulk fluorescence emission of rinsed cell supernatant (Figure S6), signifying the presence of particles not accumulated in F4/80-postive cells.

Bisphosphonate-functionalized nanogels exhibited significant localization to the external HA in the marrow-bone interface in cryosectioned spinal and femoral tissue (Figure 4d, S7–S10). Un-targeted nanogels in both femur and spine distributed throughout the marrow without localizing to the marrow-bone interface. Within the femur, the localization of targeted nanogels at the interface was apparent in both cortical and trabecular bone (Figure 4e, S11–S12). The binding of bis-nanogels to newly-synthesized HA is suggested by the co-localization of bis-nanogels with the calcium ion-binding dye calcein in femur (Figure 4f, S13).

The apparent unchanging femoral localization of targeted nanogels in Figure 4b is likely caused by the large relative volume of marrow within the femur as well as the low surface area of the marrow-bone interface. Although the targeting ligand did not increase total nanogel signal in the femur, it did shift the femoral distribution in the bone from the marrow to the HA on the external parts of the cavity, resulting in greater bone localization of the targeted nanoparticles. This may be due both to the targeting ability of the functionalized particle as well as the F4/80-postive cell depletion effect of the ligand, resulting in less nanogel sequestration in phagocytes. Localization in spine exhibited an overall increase possibly due to the cancellous nature of the spinal vertebrae with a higher surface area-to-volume ratio of the marrow-bone interface in spine versus femur, allowing a larger percentage of the nanogels in the marrow cavities to bind to spinal versus femoral bone.

Modular, dextran-based nanogels were synthesized via a facile method to improve control over chemistry, characterization, and accumulation in frequent metastatic sites. The nanogels demonstrated degradability and displayed ligands for post-functionalization via click chemistry. The particles exhibited extremely low cytotoxicity in vitro, higher uptake by macrophages versus hepatocytes and epithelial cells, and were tolerated at high doses in vivo. Biodistribution studies showed significant localization in the liver and cervical lymph nodes, and bone marrow F4/80-postive cells uptake. Functionalization with a bisphosphonate ligand modulated this localization, reducing kidney and liver uptake by 43% and increasing accumulation in the spine by 36%. The targeting ligand resulted in significant nanogel localization at the HA-marrow interface in the walls of the marrow cavities in both femur and spine, and in both cortical and trabecular bone. Although the overall nanogel uptake into F4/80-postive cells was lower for the targeted nanogels, these nanogels depleted F4/80-positive cells within bone marrow, suggesting that the particles may contribute to a depletion of future ostoeclasts and might provide an anti-osteoporotic effect, which warrants further study. In summary, we demonstrated a facile technique to generate modular nanogels with controllable functionalization and targeting which hold potential for therapeutic applications towards bone disease.

Experimental

Nanogels were synthesized in an inverse miniemulsion created using 573 mg of Span™ 80 dissolved in 15 mL cyclohexane in a glass vial with a magnetic stir bar. The aqueous phase consisted of 0.043 mg/mL of alkyne-dextran polymer, 0.014 mg/mL azide-dextran polymer, 40 mM sodium ascorbate, and 13 mM of copper(II) sulfate dissolved in water. The aqueous phase was mixed immediately, after the addition of solutes, with the oil phase and ultrasonicated in a water bath for 30–60 seconds. The reaction mixture was stirred at 350 rpm for 12–20 hours.

The nanogels were purified by centrifuging the minemulsion at 16,000 rcf for 30 minutes before removing the supernatant. The pellet was resuspended in THF and centrifuged again and the supernatant was removed. The pellet was then suspended in water and dialyzed extensively using a 100,000 MWCO membrane for four days. Particles were lyophilized and stored at −20 °C. Additional methods are found in the Supporting Information.

Supplementary Material

Refer to Web version on PubMed Central for supplementary material.

Acknowledgments

The authors would like to thank O. Z. Fisher, Y. Zhang, and D. J. Siegwart for useful discussions. This work was supported by NIH RO1 DE016516, NIH R01 EB000244, and the Damon Runyon Cancer Research Foundation (DFS-#2050-10).

References

1. Wang D, Miller SC, Kopeckova P, Kopecek J. Advanced Drug Delivery Reviews. 2005; 57:1049. [PubMed: 15876403] Zhang SF, Gangal G, Uludag H. Chem Soc Rev. 2007; 36:507. [PubMed: 17325789]
2. Kabanov AV, Vinogradov SV. Angew Chem Int Edit. 2009; 48:5418.Naeye B, Deschout H, Roding M, Rudemo M, Delanghe J, Devreese K, Demeester J, Braeckmans K, De Smedt SC, Raemdonck K. Biomaterials. 2011; 32:9120. [PubMed: 21890194] Raemdonck K, Demeester J, De Smedt S. Soft Matter. 2009; 5:707.Zhan FX, Chen W, Wang ZJ, Lu WT, Cheng R, Deng C, Meng FH, Liu HY, Zhong ZY. Biomacromolecules. 2011; 12:3612. [PubMed: 21905663] Oh JK, Drumright R,

Siegwart DJ, Matyjaszewski K. Prog Polym Sci. 2008; 33:448.Vinogradov SV, Bronich TK, Kabanov AV. Advanced Drug Delivery Reviews. 2002; 54:135. [PubMed: 11755709]

3. Robinson MJ, Sancho D, Slack EC, LeibundGut-Landmann S, Reis e Sousa C. Nat Immunol. 2006; 7:1258. [PubMed: 17110942]
4. Van Thienen TG, Lucas B, Flesch FM, van Nostrum CF, Demeester J, De Smedt SC. Macromolecules. 2005; 38:8503.
5. Tamura M, Ichinohe S, Tamura A, Ikeda Y, Nagasaki Y. Acta Biomater. 2011; 7:3354. [PubMed: 21664304]
6. Lawson MA, Xia Z, Barnett BL, Triffitt JT, Phipps RJ, Dunford JE, Locklin RM, Ebetino FH, Russell RG. J Biomed Mater Res B Appl Biomater. 2010; 92:149. [PubMed: 19904734]
7. Deligny CL, Gelsema WJ, Tji TG, Huigen YM, Vink HA. Nucl Med Biol. 1990; 17:161.
8. Wong R, Wiffen PJ. Cochrane Database Syst Rev. 2002:CD002068. [PubMed: 12076438] Fleisch H. Eur Spine J. 2003; 12:S142. [PubMed: 13680318]
9. Gittens SA, Bansal G, Zernicke RF, Uludag H. Advanced Drug Delivery Reviews. 2005; 57:1011. [PubMed: 15876401] Uludag H, Kousinioris N, Gao TJ, Kantoci D. Biotechnol Prog. 2000; 16:258. [PubMed: 10753453] Uludag H. Curr Pharm Design. 2002; 8:1929.
10. Low SA, Kopecek J. Adv Drug Deliv Rev. 2012; 64:1189. [PubMed: 22316530]
11. Kolb HC, Sharpless KB. Drug Discov Today. 2003; 8:1128. [PubMed: 14678739]
12. Bencherif SA, Siegwart DJ, Srinivasan A, Horkay F, Hollinger JO, Washburn NR, Matyjaszewski K. Biomaterials. 2009; 30:5270. [PubMed: 19592087]
13. Nystrom AM, Bartels JW, Du W, Wooley KL. J Polym Sci Pol Chem. 2009; 47:1023.
14. Fisher OZ, Kim T, Dietz SR, Peppas NA. Pharm Res. 2009; 26:51. [PubMed: 18751960]
15. Smith MH, South AB, Gaulding JC, Lyon LA. Anal Chem. 2010; 82:523. [PubMed: 20000662]
16. Kobayashi H, Koyama Y, Barrett T, Hama Y, Regino CA, Shin IS, Jang BS, Le N, Paik CH, Choyke PL, Urano Y. Acs Nano. 2007; 1:258. [PubMed: 19079788]
17. Vasquez KO, Casavant C, Peterson JD. PLoS One. 2011; 6:e20594. [PubMed: 21731618]
18. Lean JM, Matsuo K, Fox SW, Fuller K, Gibson FM, Draycott G, Wani MR, Bayley KE, Wong BR, Choi Y, Wagner EF, Chambers TJ. Bone. 2000; 27:29. [PubMed: 10865206]
19. Fisher JE, Rogers MJ, Halasy JM, Luckman SP, Hughes DE, Masarachia PJ, Wesolowski G, Russell RG, Rodan GA, Reszka AA. Proc Natl Acad Sci USA. 1999; 96:133. [PubMed: 9874784]
20. Moreau MF, Guillet C, Massin P, Chevalier S, Gascan H, Basle MF, Chappard D. Biochem Pharmacol. 2007; 73:718. [PubMed: 17157266] Delmas PD. Curr Opin Rheumatol. 2005; 17:462. [PubMed: 15956844]

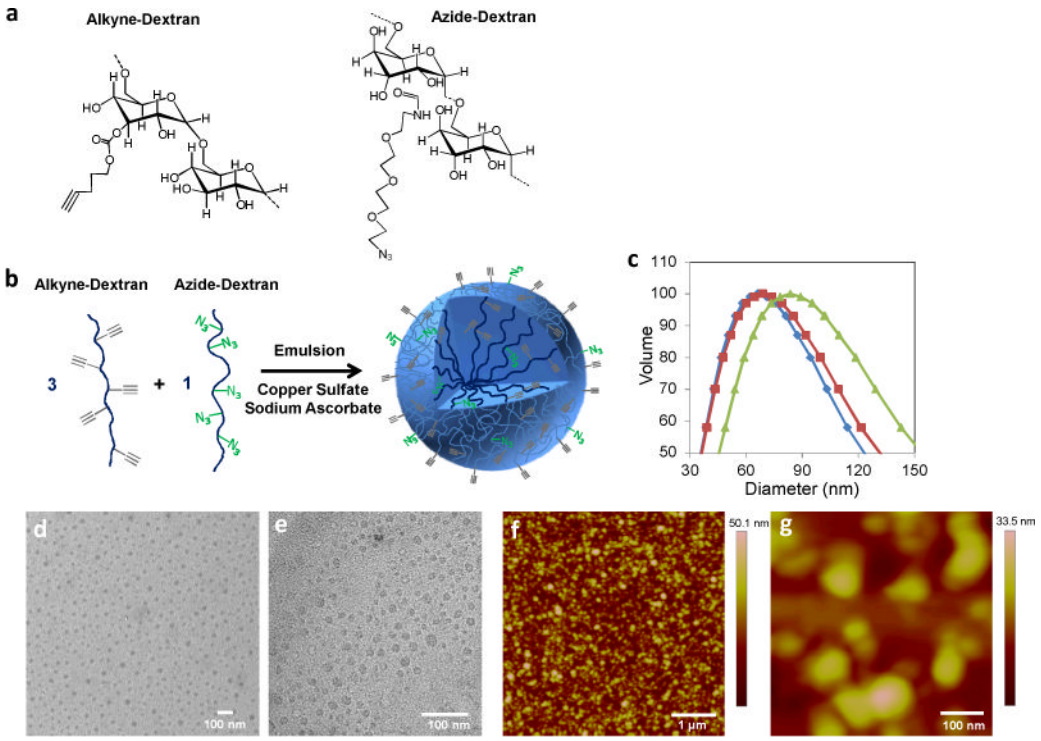

Figure 1.

(a) Dextran polymer precursors with alkyne or azide ligands for click chemistry. (b) Synthesis scheme for alkyne-heavy nanogels: alkyne and azide –functionalized dextrans react within an inverse emulsion. (c) DLS measurements of alkyne-heavy (♦), bisphosphonate-functionalized (■), and azide-heavy (▲) nanogels in PBS. (d–e) Transmission electron micrographs of alkyne-heavy nanogels. (f–g) Atomic force micrographs of surface-bound alkyne-heavy nanogels. Microscopy was conducted in dry conditions.

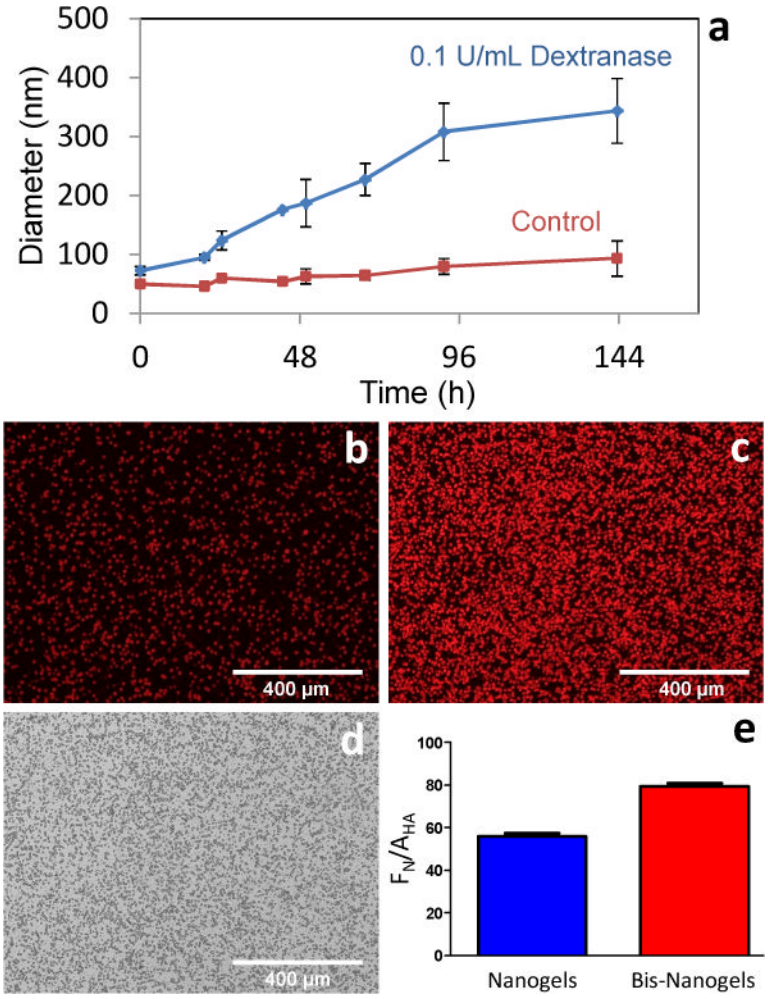

Figure 2.

(a) Dextranase degradation of nanogels at pH 6.0. Nanogel size increases approximately 500%. All error bars equal one standard deviation. (b) Fluorescently-labeled alkyne-heavy nanogel and (c) bisphosphonate-derivatized nanogel binding study to surface-bound hydroxyapatite particles. (d) Bright-field image of hydroxyapatite particles. (e) Fluorescence of nanogels (F_N) measured relative to hydroxyapatite particle area (A_{HA}).

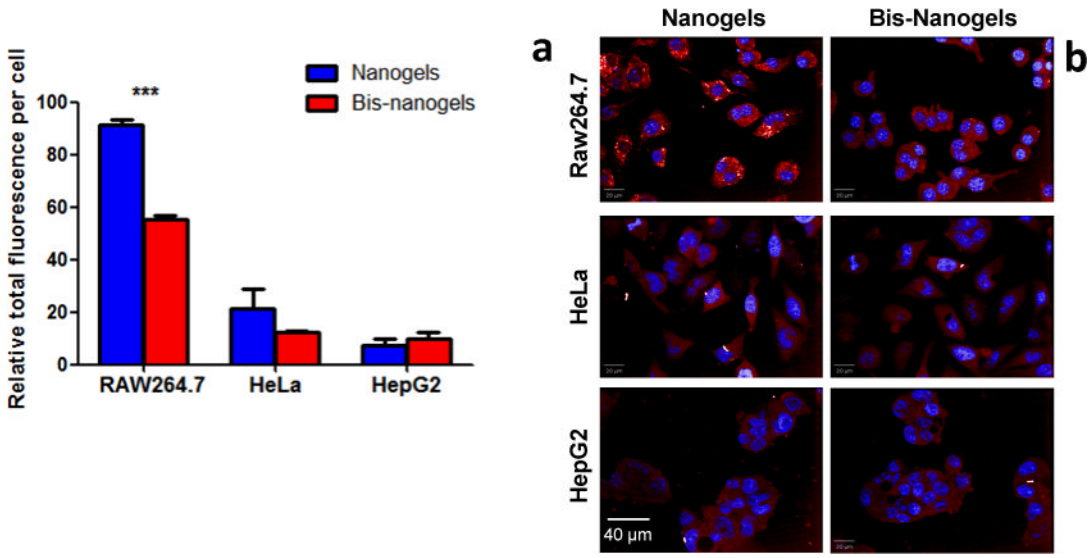

Figure 3.

Alkyne-heavy nanogels exhibit enhanced uptake by RAW 264.7 macrophages compared to HeLa and HepG2 cells. (a) Quantitated total fluorescence in three cell types computed from (b) images of fluorophore-labeled nanogels taken with a high-throughput confocal fluorescence microscopy system. Asterisks signify that means are significantly different ($P<0.0001$)

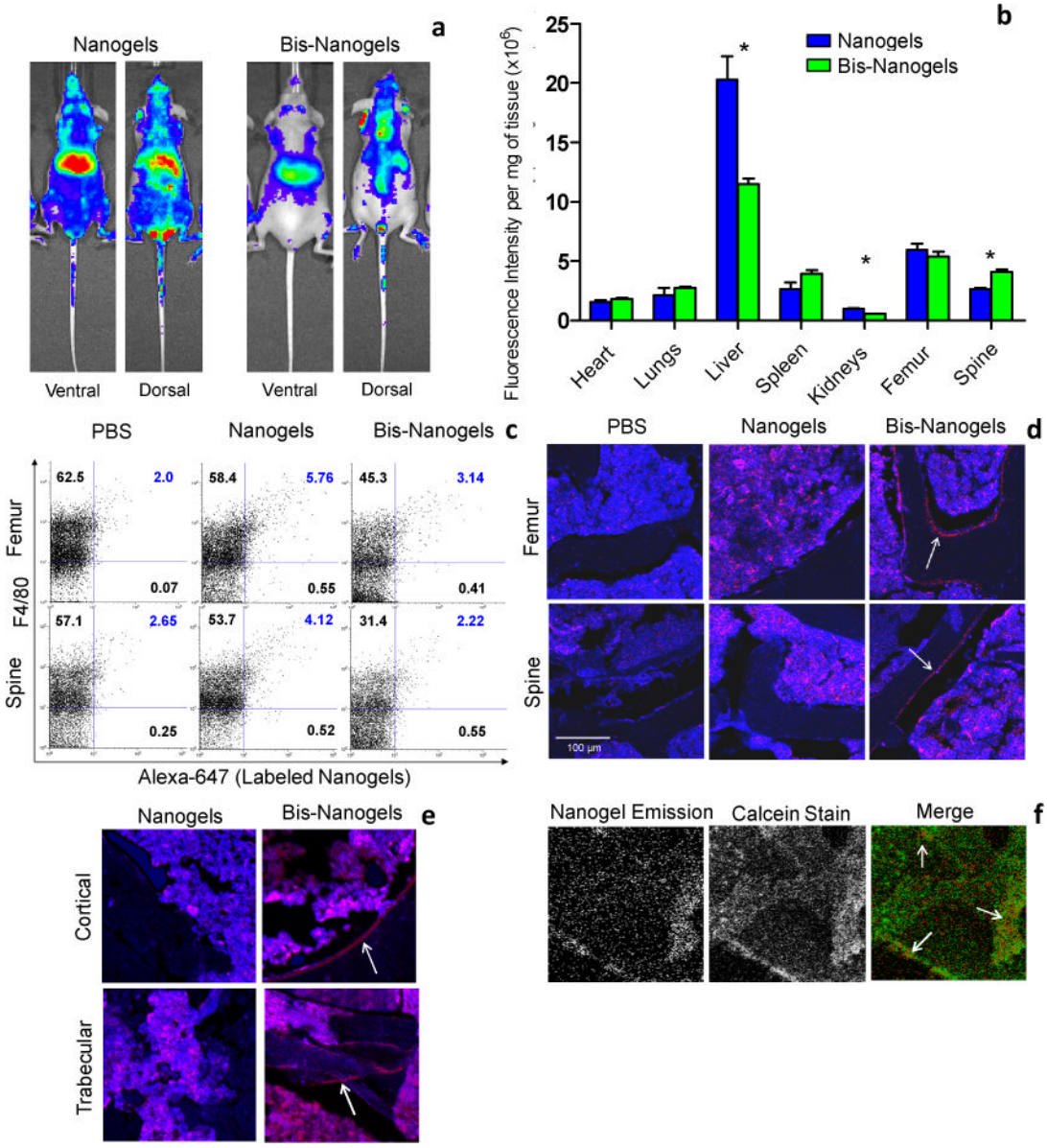

Figure 4.

Biodistribution of alkyne-heavy nanogels and bisphosphonate-functionalized nanogels (Bis-Nanogels) in SKH-1 hairless mice. (a) In vivo fluorescence at 24 hours. Liver and lymph node localization is evident in the ventral view, while the dorsal view shows increased relative spinal distribution of bis-nanogels. (All mice shown in Figure S2, N=4.) (b) Relative fluorescence intensity in organs ex vivo, after 24 hours. Asterisks signify that means are significantly different ($P<0.05$). (c) FACS analysis of $F4/80^+$ and co-positive $F4/80^+Alexa\text{-}647^+$ cells in single-cell suspensions prepared from PBS- or nanoparticle- (nanogels or bis-nanogels) treated bone marrow (spinal or femural) from SHK-1 mice. Cell numbers shown in each quadrant are expressed as a percentage of the total cell population. In correlation with in vitro data (Figure 3), bisphosphonate modification decreased F4/80/Alexa-647 co-positive cell populations in spine and femur bone marrow *in vivo* by 46.2% and 45.5%, respectively, as compared to Dex-treated samples (n=2 per treatment group). (d) Confocal images of cryosectioned femur and spinal vertebrae treated with either PBS,

nanogels, or bis-nanogels, and isolated from SHK-1 mice at 24 hr. Representative images taken with a 10X objective lens are shown for both femurs and spine. Nanogel signal (Alexa-647) is shown in red. Bone marrow and bone morphological features are shown in blue. White arrows highlight the bis-nanogel-bound bone tissue. (e) Cryosections cortical and trabecular femoral bone tissue are shown after treatment with either nanogels or bis-nanogels. White arrows highlight bis-nanogel bound bone. (f) Calcein-stained femur shows areas of co-localization of bis-nanogel fluorescence and higher calcium concentrations in the tissue.